



# Highly redox bio-based polyazomethines: synthesis and studies on their electrochemical behavior

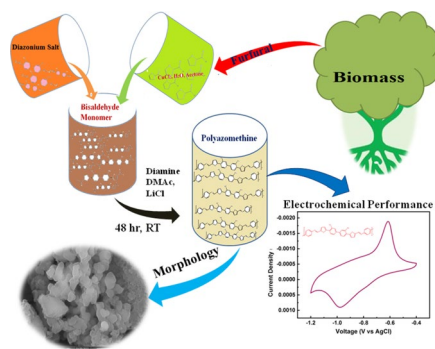
Amburaya S. Birajdar<sup>1</sup> · Shailesh G. Pawar<sup>2</sup> · Anil A. Ghanwat<sup>3</sup> · Vijaykumar P. Ubale<sup>1</sup>

Received: 30 May 2023 / Accepted: 7 November 2023 / Published online: 26 December 2023  
© Iran Polymer and Petrochemical Institute 2023

## Abstract

The highly redox semi-conducting polyazomethine films have been produced at room temperature using a bio-based furfuraldehyde moiety on a stainless steel (SS) substrate. Polyazomethines are alternatively conjugated polymers with backbones made of different furan-based aromatic rings. New monomer, 5-{4-[4-(5-formylfuran-2-yl)-3-methylphenyl]-2-methylphenyl} furan-2-carbaldehyde (III), has been synthesized by coupling reaction. The structure of monomer has been confirmed by spectroscopic techniques. Aromatic diamines, viz., 1,4-phenylene diamine, 4,4'-diaminodiphenyl ether, *o*-tolidine, 1,2-phenylene diamine, and 1,5-naphthalene diamine, with this novel monomer (III) have achieved a new series of polyazomethine (OTD-1 to OTD-5). A Fourier transform infrared (FTIR) investigation revealed the  $-C=N$  linkage. XRD analysis of polymers has confirmed their amorphous nature. Granular morphology is observed using FESEM. The constituents of polyazomethine (C, N, and O) have been confirmed by EDAX. The electrochemical performances of the prepared polyazomethines have been examined by cyclic voltammetry (CV), galvanostatic charge–discharge (GCD), and electrochemical impedance spectroscopy (EIS). Polyazomethines synthesized by polycondensation of bisaldehyde monomer (III) and 4,4'-diaminodiphenyl ether named OTD-2 showed optimum electrochemical performance, bearing the highest specific capacitance ( $C_p$ ) of 272.36 F  $g^{-1}$ , specific energy (SE) (6.06 Wh  $kg^{-1}$ ), and specific power (SP) (16.20 kW  $kg^{-1}$ ) in 0.5 M NaOH electrolyte. The stability of OTD-2 was found to be 71.25% after 1000 cycles.

## Graphical abstract



**Keywords** Bisaldehyde · Polyazomethines · Conductivity · Electrochemical studies · Impedance

✉ Vijaykumar P. Ubale  
vpubale@gmail.com

- <sup>1</sup> Department of Chemistry, D. B. F. Dayanand College of Arts and Science, Solapur 413002, India
- <sup>2</sup> Department of Physics, D. B. F. Dayanand College of Arts and Science, Solapur 413002, India
- <sup>3</sup> Polymer Research Laboratory, School of Chemical Sciences, PAH Solapur University, Solapur 413255, India

## Introduction

In the past 2 decades, researchers have shown significant interest in bio-based polyazomethines, or poly(Schiff-base), attributable to their unique characteristics, viz., crystallinity, elevated thermal strength, metal-chelating ability, and

outstanding mechanical properties [1]. Aromatic polyazomethines, in particular, exhibit special optoelectrical conductivity and have the potential for valuable applications in optoelectrical fields [2, 3]. Polyazomethines are used in different applications like supercapacitor electrodes, battery cathodes, electronic devices, electrochromic displays, etc. [4, 5]. The supercapacitor utilizes energy accumulators based on various resources like carbon species, metals, and conjugated polymers [6]. Electrode materials utilizing carbon derivatives of high stability and conductivity tend to exhibit EDLC behavior with extraordinary power density and improved cycling stability [7]. Nonetheless, because of the energy storage method in capacitors, the energy density is constrained [8]. Electrodes of metal oxide exhibit a pseudocapacitive nature with prominent energy storage in a supercapacitor due to their exceptional redox activity, excluding challenges such as low conductivity and high cost. The boundaries of carbon and metal oxide electrodes widened with the utilization of conjugated polymers like polypyrrole, polyaniline (PANi), and polyazomethine due to their easy processing, high energy density, light weight, high conductivity, less toxicity [9], and environmental friendliness [10]. The process of preparing polyazomethines is a simple polycondensation of diamine and bisaldehyde monomers through simultaneous H<sub>2</sub>O delivery [11]. The polyazomethine based on furan moiety was synthesized by altering the monomer functional groups like phenyl, furan, ester, ether, silane, thiophene, ferrocene, pyridine, triazole, and others. Through derivatization, various polyazomethine types can be conveniently produced. Nevertheless, azomethine polymerizations have been synthesized in various solvents, viz., dimethylformamide (DMF), dimethylsulfoxide (DMSO), hexamethyl phosphoramide (HMPA), *N*-methylpyrrolidone (NMP), and dimethylacetamide (DMAc) [12]. Furaldehyde and its derivatives are usually extracted from agricultural waste, such as oat hulls, corn cobs, and bagasse [13–15]. The redox behavior of polyazomethines is customized with changing conjugated heterocyclic aromatic moiety and interconversion of various functional groups [16–19].

In recent years, researchers have shown interest in the synthesis and applications of semi-conducting conjugated polymers like polyazomethines. Li et al. [20] have brilliantly evaluated polyazomethines synthesized at 200 °C for 1 h using microwave-assisted hydrothermal method. Yuya et al. [21] have excellently prepared poly(Schiff-base) at 140 °C for 6 h via polycondensation method. Summarizing previously reported synthesis of polymers by various polymerization methods were carried at elevated temperature. Conversely, we report here the synthesis of the bio-based monomer 5-{4-[4-(5-formylfuran-2-yl)-3-methylphenyl]-2-methylphenyl}

2-methylphenyl} furan-2-carbaldehyde (III) and its use in the preparation of polyazomethines by the polycondensation process at room temperature for 24 h. A series of polyazomethines was prepared by condensing bisaldehyde monomer with various diamine monomers toward extensive evaluation of supercapacitive properties.

## Experimental

### Chemicals

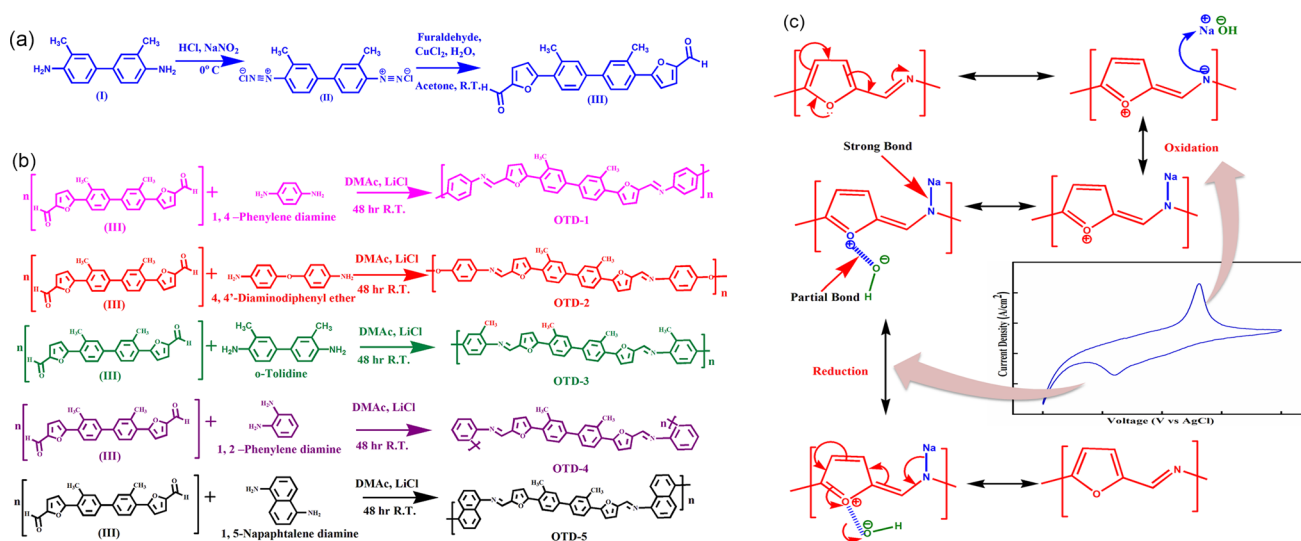
Bisaldehyde and polyazomethines were synthesized using AR-grade precursors from Avra Synthesis Pvt., Bangalore, India. NMP (Avra Synthesis Pvt., Bangalore, India 98%), DMAc (Avra Synthesis Pvt., Bangalore, India 98%), *o*-tolidine (Avra Synthesis Pvt., Bangalore, India 98%), furaldehyde (Avra Synthesis Pvt., Bangalore, India 99%), DCM (Avra Synthesis Pvt., Bangalore, India 99%), glacial acetic acid (Avra Synthesis Pvt., Bangalore, India 99%), toluene (Avra Synthesis Pvt., Bangalore, India 99%), methanol dried (Molychem Mumbai, India), tetrahydrofuran (Avra Synthesis Pvt., Bangalore, India 99%), ethanol dried, and DMAc (Avra Synthesis Pvt., Bangalore, India 98%) have been purified by the standard procedure. Anhydrous lithium chloride has been vacuum dehydrated at 80 °C for 8 h.

### Synthesis of monomer 5-{4-[4-(5-formylfuran-2-yl)-3-methylphenyl]-2-methylphenyl} furan-2-carbaldehyde (III)

5-{4-[4-(5-Formylfuran-2-yl)-3-methylphenyl]-2-methylphenyl}furan-2-carbaldehyde (III) has been synthesized in a single step with a percentage yield of 88.95 and a melting point (mp) 118 °C as shown in Scheme 1a. First, 2 mmol sodium nitrite (40 mL) was added drop-wise to 1 mmol *o*-tolidine at a temperature of 0–5 °C. The resultant solution was mixed with a 4:3 ratio of hydrochloric acid to water, and the prepared mixture which was identified as cold diazonium salt was slowly been added to a vigorously stirred 0.1 mol CuCl<sub>2</sub> 2H<sub>2</sub>O and 2 mmol furaldehyde in acetone at 25 °C. The resultant precipitate was filtered; and the impurities were removed by repeatedly washing with distilled water (DW), and dried.

### Synthesis of polyazomethine (OTD-1)

A three-neck flask with a magnetic stirrer was charged with 5-{4-[4-(5-formylfuran-2-yl)-3-methylphenyl]-2-methylphenyl} furan-2-carbaldehyde (III) (1 mmol), LiCl (3.5 mmol),



**Scheme 1** **a** Synthesis of 5-[4-[4-(5-formylfuran-2-yl)-3-methylphenyl]-2-methylphenyl] furan-2-carbaldehyde (III), **b** synthesis of  $\pi$ -conjugated aromatic polyazomethines (OTD-1 to OTD-5

from bisaldehyde (III), and **c** probable redox (charging and discharging) mechanism of polyazomethine moiety

and 5 mL dried DMAc. After the dissolution of monomer, 1,4-phenyldiamine (1 mmol) was added, and the solution was homogenized for 48 h at RT under  $N_2$  atm. Anhydrous lithium chloride has been utilized as a water scavenger. The viscous dark brown polyazomethine (OTD-1) was precipitated by pouring in methanol–water (50:50) and washed three times with methanol–water (50:50), warm water, and acetone. The resulting dark brown polyazomethine was desiccated at 80 °C (Scheme 1b).

Similarly, polyazomethines (OTD-2 to OTD-5) were prepared by following the same procedure using bisaldehyde (III) and different diamines. All polymers were obtained in quantitative yield.

## Characterization

Structure of monomer (III) has been confirmed by Fourier transform infrared (FTIR),  $^1H$  NMR, and  $^{13}C$  NMR. The FTIR Thermo Nicoletis-10 Mid spectrometer was used for chemical composition analysis of polyazomethines with recorded values in the range of 500–4000  $cm^{-1}$ . The amorphous structure has been confirmed with Bruker D8 XRD  $CuK\alpha$  ( $\lambda = 1.5406 \text{ \AA}$ ) radiation in  $2\theta$  range of 0°–80°. Surface morphology and elemental composition of the products have been observed by field emission scanning electron microscopy (FESEM, Model Jeol-6300F) with energy-dispersive X-ray spectroscopy (EDAX). A CHI 608E electrochemical analyzer has been utilized to check the electrochemical performance. The working electrode was polyazomethines coated on stainless steel plates; the counter electrode was a platinum wire; and the reference electrode is Ag/AgCl.

## Results and discussion

### Monomer characterization

The monomer was identified using FTIR spectroscopy shown in Fig. 1a, which the aldehyde carbonyl functional group ( $-C=O$ ) reveals vibration due to stretching, observed at 1666  $cm^{-1}$  and at 2924  $cm^{-1}$ , aldehyde hydrogen stretching is observed. Figure 1b reveals the  $^1H$  NMR spectrum: the chemical shift of the aldehyde proton corresponds to 9.52  $\delta$  ppm (S, 2H) and 7.20 to 7.78  $\delta$  ppm attributed to all aromatic protons; 2.37  $\delta$  ppm (S, 6H) indicates that the methyl protons are directly connected to the aromatic ring.  $^1H$  NMR spectra confirm seven types of protons in bisaldehyde monomer (III). Also, in  $^{13}C$  NMR data shown in Fig. 1c, the chemical shift at 175.4 ppm is attributed to an aldehyde carbonyl carbon, and the 158.4 to 121.9  $\delta$  ppm range shows the aromatic carbons of the monomer. A chemical shift at 108.6  $\delta$  ppm reveals the presence of methyl carbon. The monomer was confirmed by spectroscopic results [22]

### Characterization of polyazomethines

The amorphous nature of the polyazomethines has been examined using the XRD technique. In Fig. 2a, the amorphous nature of polyazomethines is confirmed by broad X-ray diffraction peaks at 5 to 18°, because no more sharp peaks have been detected [23].

The  $\pi$ -conjugated polyazomethines have been identified using FTIR spectroscopy. Figure 2b–f reveals that the imine nitrogen ( $-CH=N-$ ) stretching vibrations are near

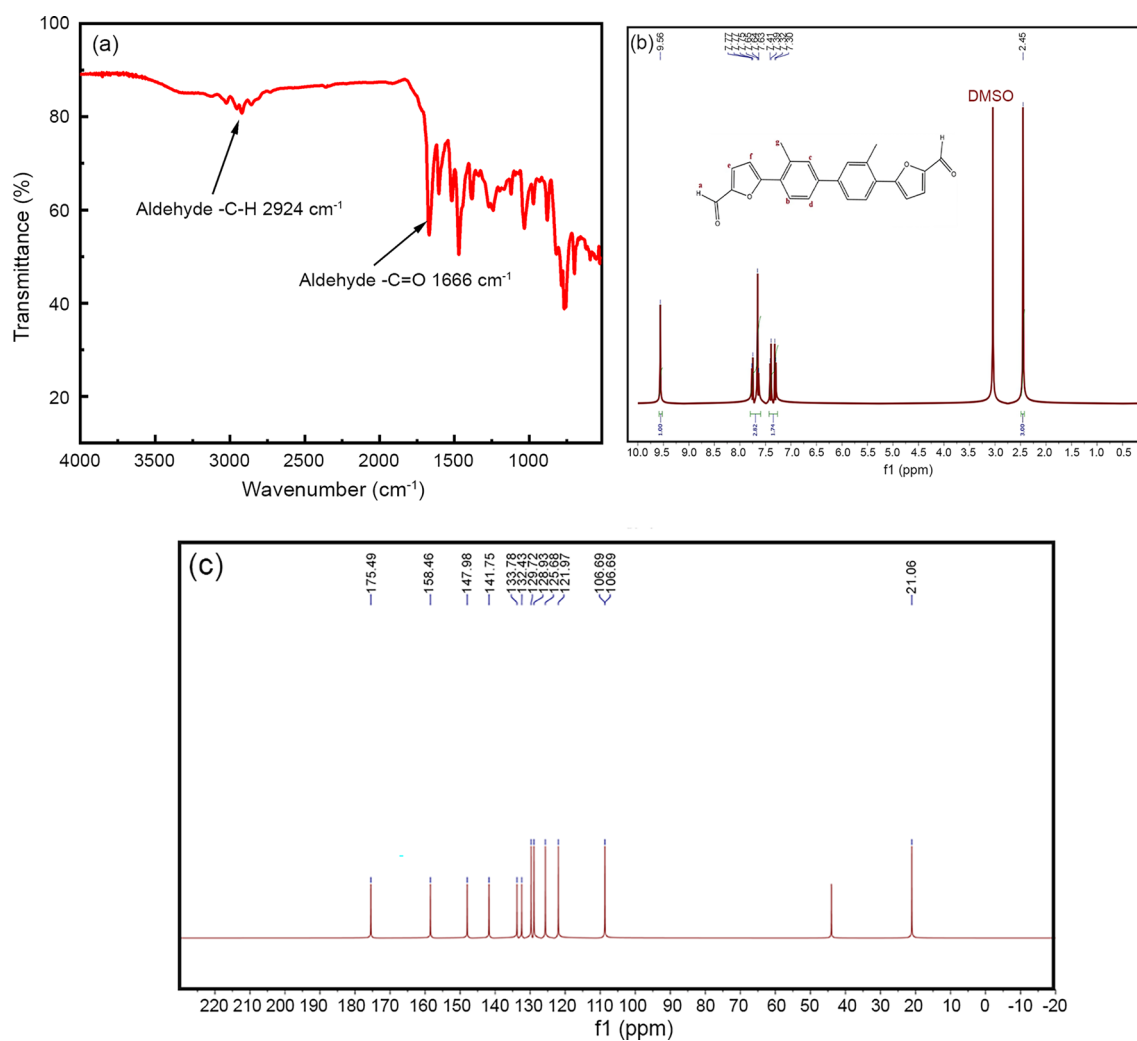


**Fig. 1** **a** FTIR spectrum of bisaldehyde, **b**  $^1\text{H}$  NMR of bisaldehyde, and **c**  $^{13}\text{C}$  NMR of bisaldehyde

$1604\text{ cm}^{-1}$ . At  $1666\text{ cm}^{-1}$ , stretching vibrations are vanished, although near  $3325\text{ cm}^{-1}$ , there is an indication that the formation of polyazomethines with bisaldehyde and diamines was to begin. The  $-\text{CH}=\text{CH}-$  stretching of frequency is thought to be responsible for absorption at  $1621\text{ cm}^{-1}$  and aromatic  $-\text{C}-\text{H}$  stretching at  $2917\text{ cm}^{-1}$ .

Figure 3a–d shows the OTD-2 electrode, which has exhibited high specific capacitance ( $C_p$ ) compared to all the samples and has been selected for morphological and compositional investigations. The FESEM micrograph for the OTD-2 thin layer has exhibited significant porosity and permeable granular shapes. The granular architecture of permeable grains is advantageous for the preoccupation of charges on the surface of thin films and can provide a superior pathway for charge mobility [24]. The EDAX spectrum of the OTD-2 thin-film electrode is shown in Fig. 4a. The results of the EDAX investigations have demonstrated the

presence of nitrogen, carbon, and oxygen. The EDAX has illustrated that carbon, nitrogen, and oxygen atoms coexist in polyazomethine, OTD-2, as shown in Fig. 4a, and it also suggests that ultra-pure polyazomethine is mainly prepared through a polycondensation route [25].

Figure 4b displays a snap of the angle of contact of  $\text{H}_2\text{O}$  on the OTD-2 electrode surface. The OTD-2 electrode surface has shown a hydrophilic nature with an angle of contact,  $31.88^\circ$  which is less than  $90^\circ$ . If the angle of contact is acute, it enhances electrochemical performance due to hydrophilic behavior [26], which in turn increases the electrolyte–electrode interfacial area of contact. The viscosity and solubility of polyazomethines have been studied in various solvents, indicating better viscosity and solubility in DMAc. Additionally, the study on electrical conductivity and thermoelectric power of OTD-2 is supplemented by supporting information.

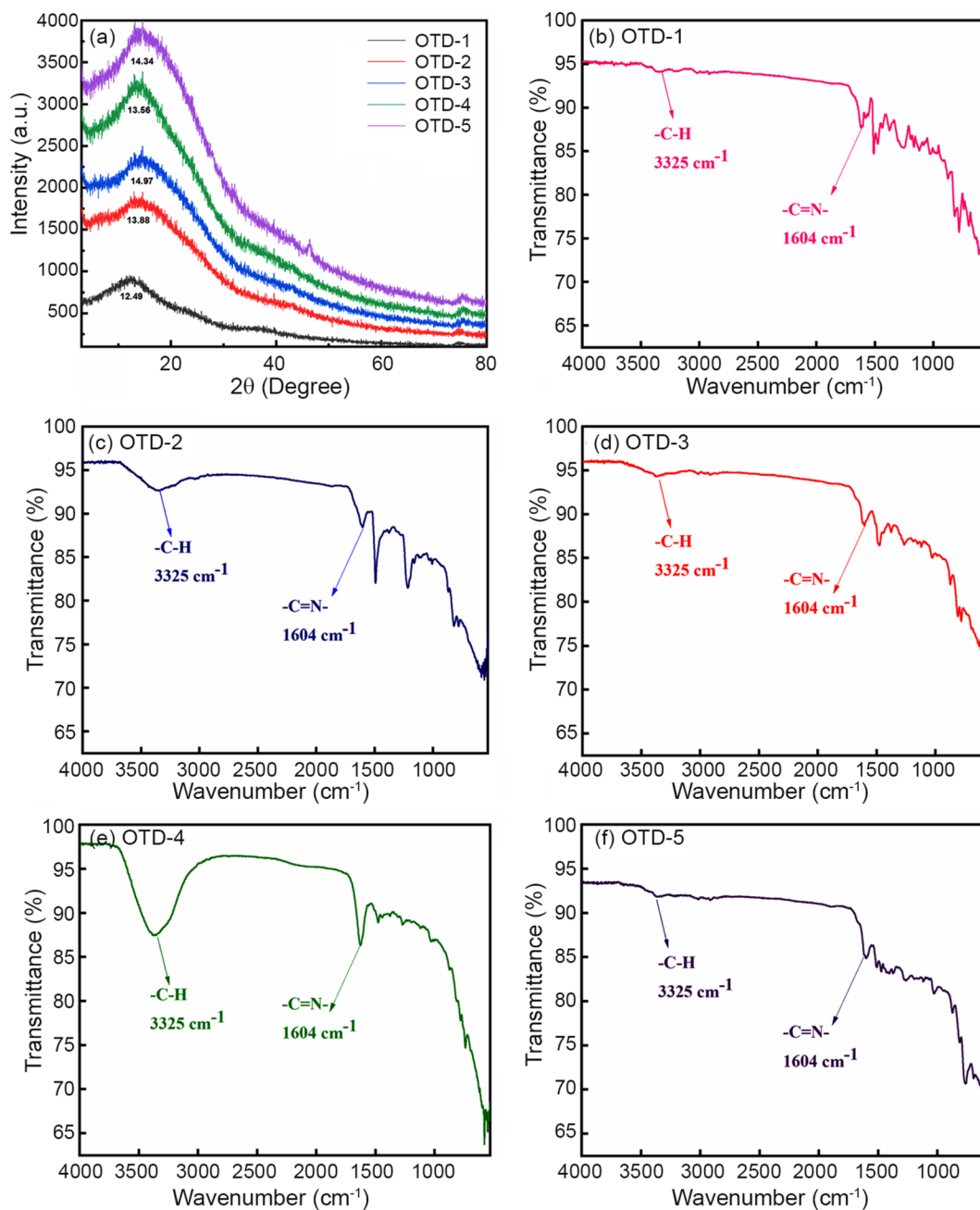


**Fig. 2** a XRD patterns of OTD-1 to OTD-5 and **b–f** FTIR spectra of OTD-1 to OTD-5, respectively

### Electrochemical measurements

A three-electrode system comprising a polyazomethine working electrode coated on stainless steel (SS) 304 grade, Ag/AgCl as a reference electrode, and platinum (Pt) wire as a counter electrode was utilized for electrochemical study. To calculate specific capacitance ( $C_p$ ) from a cyclic voltammogram, the following equation is used [27, 28]:

$$C_p = \frac{A}{2mK\Delta V}, \quad (1)$$

where  $A$  is the CV curve area,  $\Delta V$  is the window of sweep potential,  $K$  is the rate of scan (dV/dt), and  $m$  is the active mass. GCD has been used to calculate the SE, SP, and coulombic efficiency of the polyazomethine-coated supercapacitor electrode. They are calculated from the relation [29, 30]

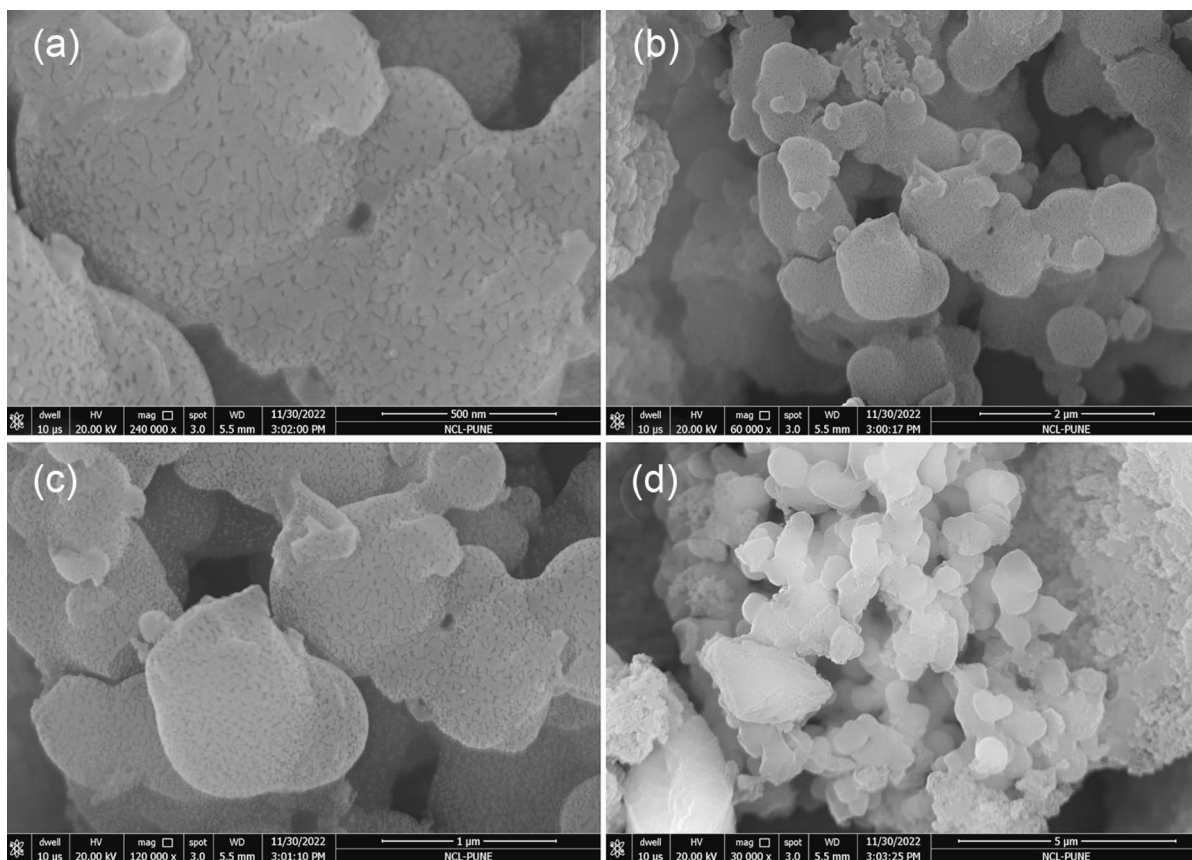
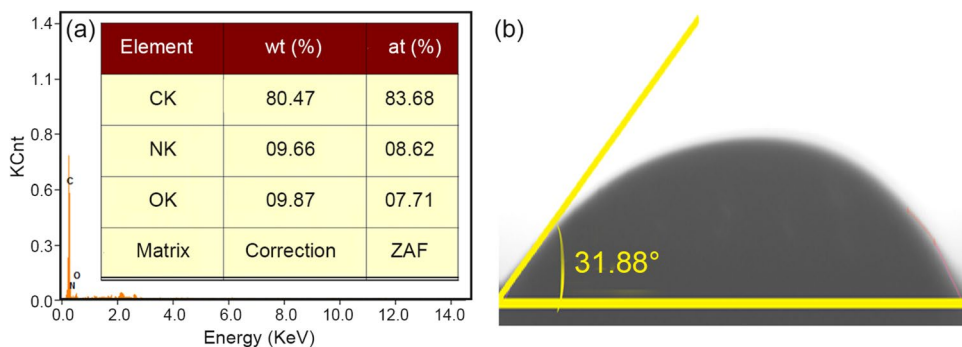


Fig. 3 FESEM images of OTD-2 at resolutions: a 0.5, b 2, c 1, and d 5 μm

Fig. 4 a EDAX of OTD-2 and b water contact angle measurement of OTD-2



$$SP = \frac{VI_d}{m} \tag{2}$$

$$SE = VI_d t_d / m \tag{3}$$

$$\eta(\%) = \frac{t_d}{t_c} \times 100, \tag{4}$$

where  $I_d$  and  $t_d$  are current density and discharge time, respectively, and  $m$  is the mass of active material within the polyazomethine electrode [31, 32].

**Optimization of polyazomethines**

All the electrodes of OTD series have been tested in 1 M NaOH by cyclic voltammetric technique at scan rates of 10 mV s<sup>-1</sup>, 20 mV s<sup>-1</sup>, 50 mV s<sup>-1</sup>, 80 mV s<sup>-1</sup>, and 100 mV

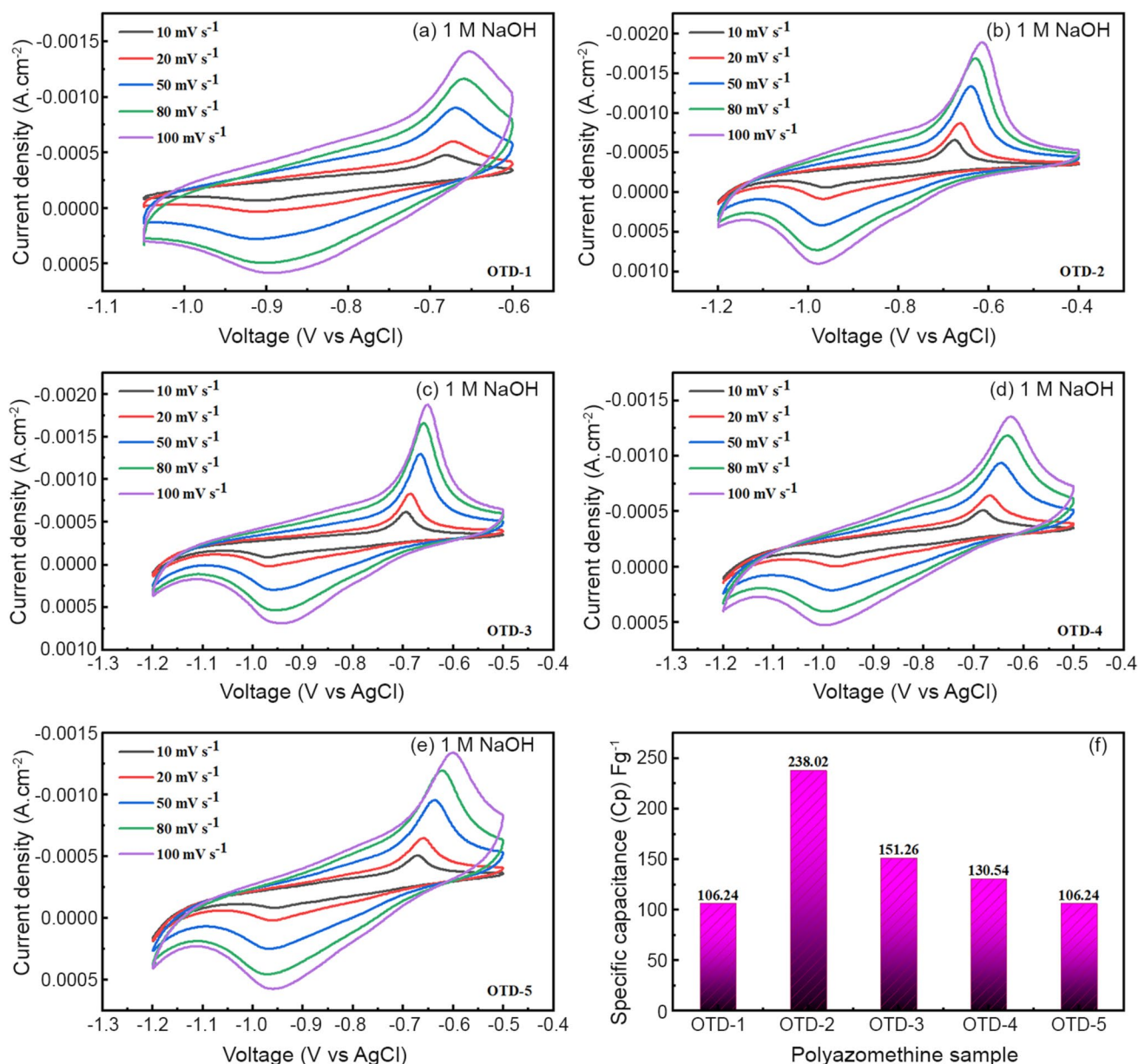


**Fig. 5** CV plots for 1 M NaOH electrolyte of OTD-1 to OTD-5 (a–e), and **f** histogram of specific capacitance ( $C_p$ ) of OTD-1 to OTD-5 at  $10 \text{ mV s}^{-1}$

$\text{s}^{-1}$  with a potential window of  $-1.2$  to  $-0.4 \text{ V}$  (Fig. 5a–e). The distinct redox peaks in all samples of the OTD series were observed, showing the redox nature of the prepared electrodes. These redox peaks are believed to arise from the oxidation and reduction of the polyazomethine, which is facilitated by a  $-\text{CH}=\text{N}-$  linkage electron-withdrawing effect, allowing the formation of polarons in the polyazomethine chain. Moreover, the redox peaks were found to shift to higher potentials with increasing the scan rates in all samples of the OTD series.

Figure 5f shows the histogram of the measured specific capacitance values of OTD series electrodes. It is evident

from the graph that the OTD-2 sample exhibits the highest specific capacitance value of  $238.02 \text{ F g}^{-1}$ . The OTD series electrodes contain bisaldehyde monomer (III) and aromatic diamines. The high  $C_p$  of OTD-2 is attributed to polymers containing co-monomer diamine (ODA) having oxygen heteroatom at *para* position of imine nitrogen. The non-bonding lone pair of electrons on the oxygen atom assists in the redox mechanism of polymers OTD-1, OTD-3, OTD-4, and OTD-5, which do not contain any extra heteroatoms assisting in the redox mechanism. The OTD-1 and OTD-4 have a single phenyl moiety, and the OTD-3 and OTD-5 have a biphenyl and naphthalene moiety, respectively.

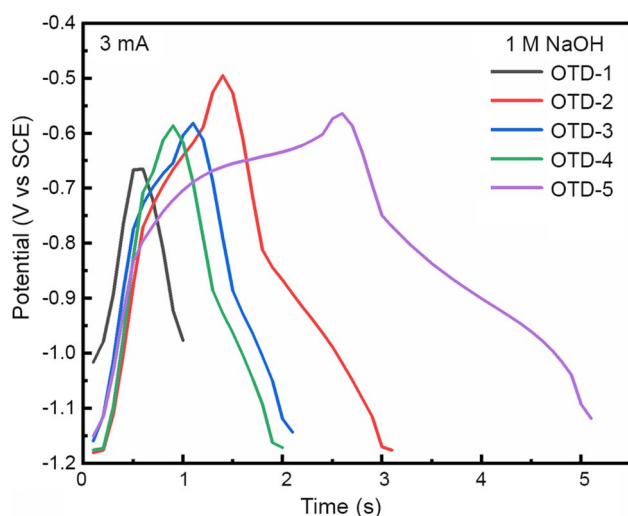


**Fig. 6** GCD curves for 1 M NaOH electrolyte OTD-1 to OTD-5 at 3 mA current density

**Table 1** Electrochemical performance of OTD-1 to OTD- 5 in 1 M NaOH

Sample	Cp (F g <sup>-1</sup> )	SE (Whr kg <sup>-1</sup> )	SP (kW kg <sup>-1</sup> )	Efficiency (%)
OTD-1	151.26	1.19	9.63	98.89
OTD-2	238.02	8.83	18.53	133.59
OTD-3	103.66	4.21	15.30	99.87
OTD-4	106.24	4.58	14.98	138.86
OTD-5	130.54	10.57	15.16	100.85

In Fig. 6, GCD plots of polyazomethines in series OTD-1 to OTD-5 at 3 mA g<sup>-1</sup> current density of all polyazomethines display an asymmetric triangular nature underlying the Faradic redox nature of polyazomethine electrodes, which is also noted by sharp oxidation and reduction peaks in the cyclic voltogram. The discharging times of all the polyazomethines were equal to or a little longer than their respective charging times. The charging and discharging times determine the efficiency of the electrode. The SE, SP, and efficiency of all the samples of polyazomethine series electrodes are calculated and summarized in Table 1. The OTD-2 sample electrode showed the Cp 238 F g<sup>-1</sup>, SE 8.83 Whr kg<sup>-1</sup>, at SP of 18.53 kW kg<sup>-1</sup>, and efficiency of 133.59%.

The optimized sample OTD-2 from the polyazomethine series was used in the subsequent study. The -1.2 V to -0.6 V potential window and scan rate of 10, 20, 50, 80, and 100 mV s<sup>-1</sup> were utilized for CV of the OTD-2 electrode in 1 M KCl, 1 M NaOH, and 1 M Na<sub>2</sub>SO<sub>4</sub> in as depicted in Fig. 7a–c, where the observed redox behavior of OTD-2 with respect to different electrolytes is shown. Figure 7d reveals the histogram of measured Cp values for the OTD-2

electrode in 1 M KCl, 1 M Na<sub>2</sub>SO<sub>4</sub>, and 1 M NaOH at a scan rate of 10 mV s<sup>-1</sup>. The OTD-2 has shown a high Cp of 238.02 F g<sup>-1</sup> in 1 M NaOH electrolyte.

The choice of optimal electrolyte for the electrochemical character of the supercapacitor is vital. The hydrated cationic radius, conductivity, and cationic mobility affect an ion substitution and determine the specific capacitance of the electrochemical system [33, 34]. The charge transfer rate depends on the conductivity and ionic mobility of the electrolyte and electrode, which alternatively determine the redox capability and specific capacitance of the electrochemical system.

The effect of electrolyte on the charging and discharging processes is evaluated from the GCD curves represented in Fig. 7e. The GCD was measured at 3 mA for 1 M KCl, 1 M Na<sub>2</sub>SO<sub>4</sub>, and 1 M NaOH electrolytes. It is observed from the graph that the discharging time is longer than the charging time, indicating columbic efficiency greater than 100%. This is due to the kinetics of the faradic surface reactions at polyazomethines [35]. The electrochemical supercapacitors parameters were measured and are tabulated in Table 2, which showed that polyazomethine OTD-2 has better performance in 1 M NaOH electrolyte. Thus, polyazomethine OTD-2 in NaOH electrolyte was employed for further study of electrolyte concentration variation.

### Optimization of electrolyte concentration

The electrochemical activity of a supercapacitor is significantly dependent on the electrolyte concentration; hence, the effect of electrolyte concentration on electrochemical performance was studied through cyclic voltogram (CV) as shown in Fig. 8a–c. The electrode's supercapacitive nature has been revealed by the faradic reaction rate at the material surface.

The variation in current density as well as area under the curve of the OTD-2 sample electrode in 0.1, 0.5, and 1 M NaOH is depicted in Fig. 8a–c, respectively. It is revealed from Fig. 8a–c that the OTD-2 electrode shows higher oxidation and reduction currents and a larger area under the curve in 0.5 M NaOH compared to other concentrations. In Fig. 8a–c, with an increase in concentration in the range of 0.1 to 0.5 M NaOH, the specific capacitance also increases from 180.6 F g<sup>-1</sup> to 272.36 F g<sup>-1</sup> because of the availability of more charges toward the redox-active linkages of OTD-2. As the concentration is increased to 1 M NaOH, Cp is reduced from 272.36 to 238.02 F g<sup>-1</sup> because of increased electrolytic concentration, which has affected the mobility and packing of charges, resulting in a reduced active surface area of OTD-2. Figure 8d reveals the histogram of measured Cp values for the OTD-2 electrode in 0.1, 0.5, and 1 M NaOH at a scan rate of 10 mV s<sup>-1</sup>. The OTD-2 has shown a high Cp of 272.36 F g<sup>-1</sup> in 0.5 M NaOH electrolyte.



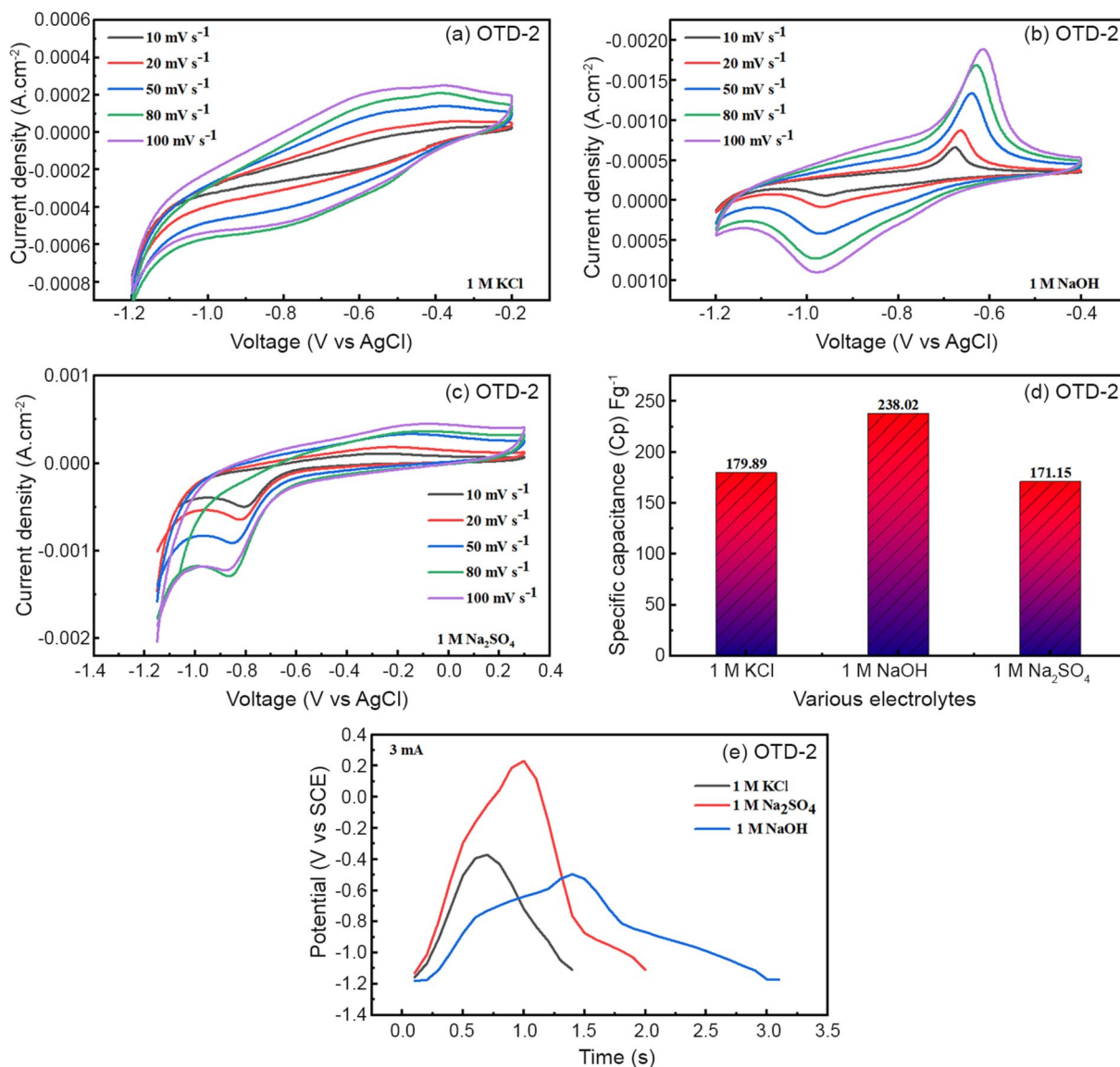


**Fig. 7** CV plots of OTD-2 in: **a** 1 M KCl, **b** 1 M NaOH, **c** 1 M Na<sub>2</sub>SO<sub>4</sub> at scan rates 10–100 mV s<sup>-1</sup>, **d** histogram of specific capacitance (Cp) of OTD-2 at 10 mV s<sup>-1</sup>, and **e** GCD curves of OTD-2 at 3 mA current density

**Table 2** Electrochemical performance of OTD-2 in various electrolytes

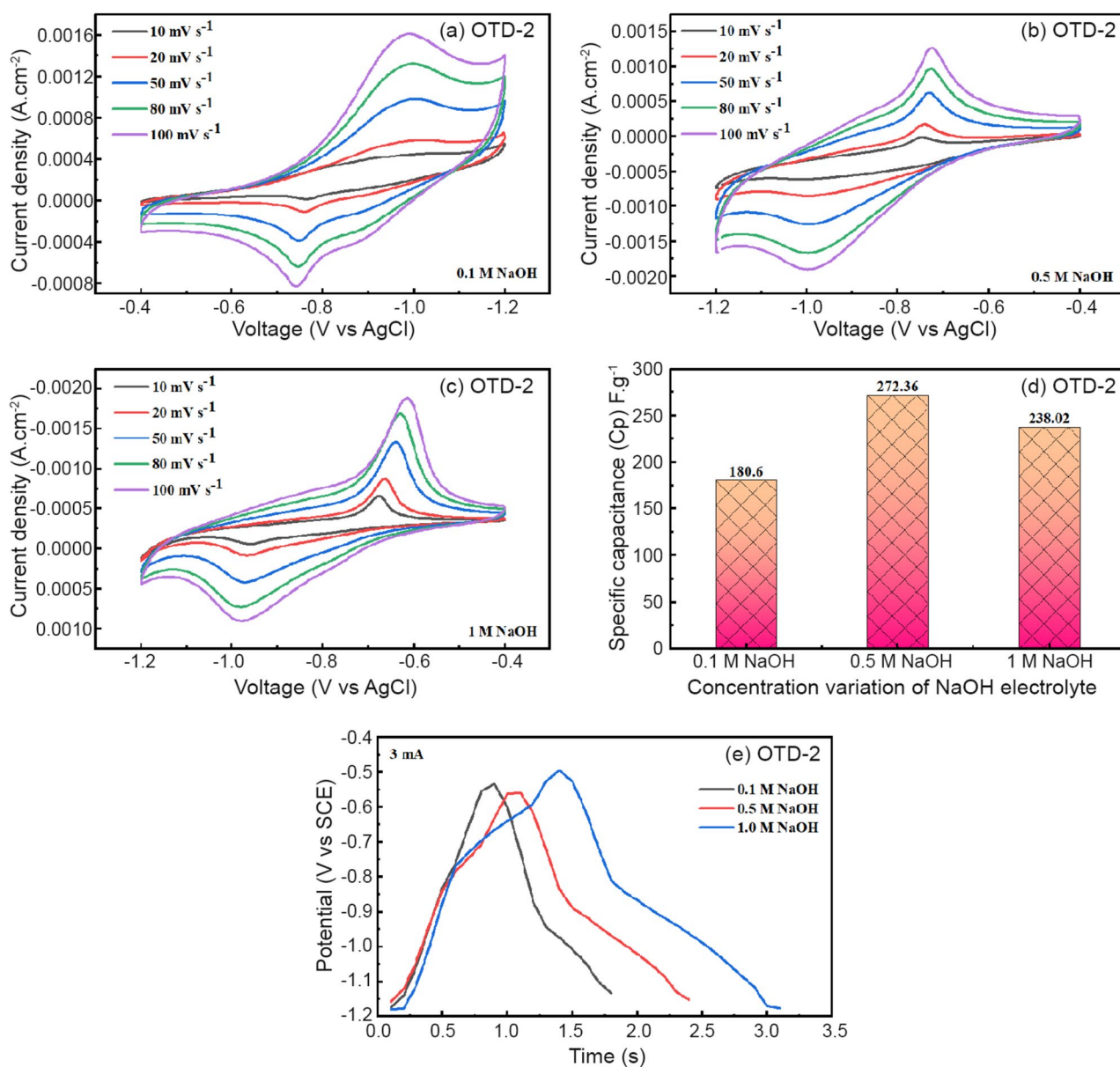
Electrolyte	Cp (F g <sup>-1</sup> )	SE (Whr kg <sup>-1</sup> )	SP (kW kg <sup>-1</sup> )	Efficiency (%)
1 M NaOH	238.02	8.83	18.53	133.59
1 M Na <sub>2</sub> SO <sub>4</sub>	171.15	6.68	23.86	111.86
1 M KCl	179.89	3.96	19.83	121.07

Figure 8e shows the GCD curves of the OTD-2 sample electrode in various concentrations of NaOH, viz., 0.1, 0.5, and 1 M of NaOH. It is demonstrated from Fig. 8e that the charging and discharging curves indicate a repeating

nature. The larger discharging time is illustrated by the probable mechanism presented in Scheme 1c. The various characteristics of the OTD-2 electrode, like Cp, CE, SP, and coulombic efficiency, are summarized in Table 3. Evidently, Tables 1, 2, and 3 reveal that the OTD-2 electrode in 0.5 M NaOH shows optimum supercapacitor performance. The real-time practical application of supercapacitors demands superior electrochemical stability.

**Stability study**

The OTD-2 electrode has shown excellent cycling stability and significantly retained specific capacitance in 0.5 M NaOH at the scan rate of 100 mV s<sup>-1</sup> tested for 1000 cycles,



**Fig. 8** CV plots of OTD-2 at various electrolyte concentrations: **a** 0.1, **b** 0.5, **c** 1 M NaOH at scan rates 10–100 mV s<sup>-1</sup>, **d** histogram of specific capacitance (Cp) of OTD-2 in various electrolyte concentrations

at scan rate 10 mV s<sup>-1</sup>, and **e** GCD curves of OTD-2 in various electrolyte concentrations at current density of 3 mA

**Table 3** Electrochemical performance of OTD-2 in various electrolyte concentrations of NaOH electrolyte

NaOH concentration (M)	Cp (F g <sup>-1</sup> )	SE (Whr kg <sup>-1</sup> )	SP (kW kg <sup>-1</sup> )	Efficiency (%)
1.0	238.02	8.83	18.53	133.59
0.5	272.36	6.06	16.20	139.96
0.1	180.60	4.07	16.20	113.28

as shown in Fig. 9a. As depicted in Fig. 9b, the sharpness of redox peaks and area under the curve are greater for the 1st cycle than the 1000th cycle. Since successive charging and discharging deplete an active material from the substrate, from the obtained result, lone pair of electron on hetero-oxygen has enhanced the supercapacitor performance of OTD-2, which makes it a promising functional material for high-performance supercapacitor electrodes. Furthermore, we have conducted a comparative analysis of our findings with results reported in the literature for various materials

**Fig. 9** **a** Stability of OTD-2 at scan rate of  $100 \text{ mV s}^{-1}$  at 1st and 1000th cycle in 1 M NaOH and **b** stability performance of OTD-2

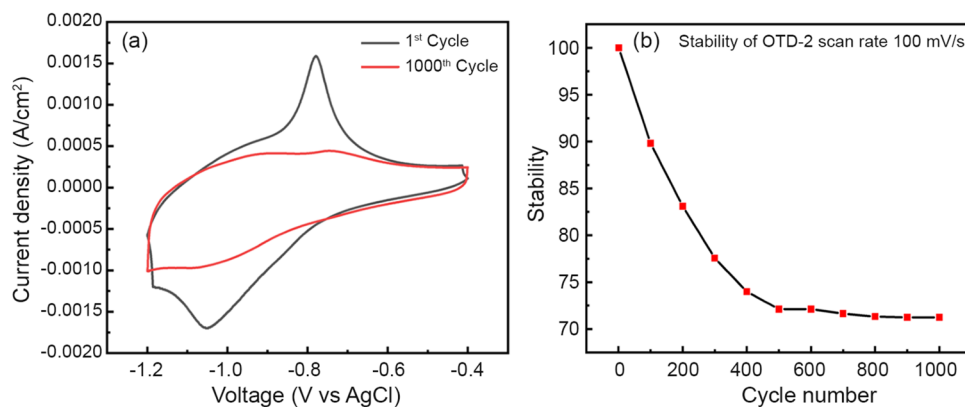


**Table 4** Specific capacitance of different polymers/polymer hybrids in various electrolytes

Material	Specific capacitance ( $\text{F g}^{-1}$ )	Electrolyte	Number of cycles	Cyclic stability (%)	References
Porous	129.5	1 M NaOH	1500	–	[36]
Polyaniline, $\text{MnO}_2$ , $\text{Ti}_3\text{C}_2\text{Tx}$ MXene	21.1	PVA/ $\text{H}_2\text{SO}_4$	4000	83	[37]
Polyaniline, $\text{MnO}_2$ , $\text{MoS}_2$	259	0.2 M $\text{H}_2\text{SO}_4$	4000	75.94	[38]
Polyaniline, $\text{RuO}_2$ , $\text{TiO}_2$	67.4	0.1 M $\text{H}_2\text{SO}_4$	10,000	81.6	[39]
Polyaniline, $\text{WO}_3$	180	–	10,000	70	[40]
Polyaniline, $\text{MoO}_3$ , $\text{SiO}_2$ , mesoporous carbon (MC)	45	1 M $\text{H}_2\text{SO}_4$	250,000	57	[41]
Polypyrrole, $\text{MnO}_2$ , Carbon cloth	270	–	3000	92.1	[42]
Polypyrrole, ZnO	161.02	1 M KCl	5000	70.71	[43]
Poly(3,4 ethylene dioxythiophene), $\text{MnO}_2$ , $\text{V}_2\text{O}_5$	116.9	Carboxymethyl cellulose sodium (CMC)- $\text{Na}_2\text{SO}_4$ gel	10,000	87.2	[44]
OTD-2	272.36	0.5 M NaOH	1000	71.25	This work

in the context of supercapacitor research, which is organized into Table 4.

### EIS study

The charge transfer and ion diffusion mechanisms can be investigated through EIS measurements [45]. Therefore, the EIS technique was utilized to study the supercapacitive nature of the OTD-2 sample. Figure 10a shows the Nyquist plot of OTD-2 in the range from 10 kHz to 0.1 Hz in a 0.5 M NaOH electrolyte.

Usually a semi-circle on the left of the graph intercepts the real ( $Z'$ ) axis attributed to resistance  $R_s$  ( $1.23 \Omega$ ), within the electrolyte and electrode, which is identical with the sum of contact resistance and the internal resistance of the material. Figure 10a depicts the absence of such a semi-circle, showing a negligible charge transportation resistance within the electrolyte and electrode and, accordingly, the least impact of the capacitive double layer. Thus, the redox behavior of OTD-2 is responsible for the pseudocapacitor nature of the OTD-2 electrode. An electrical equivalent

circuit obtained from impedance fitting is shown in the inset of Fig. 10a. A series resistance  $R_s$  is connected to the constant phase element (CPE) ( $0.0003425 \text{ S.s}$ ), which is the pseudocapacitor component, in parallel with the charge transfer resistance  $R_{ct}$  ( $919.2 \Omega$ ). Figure 10b of the spider diagram of OTD-2 shows the electrochemical parameters specific capacitance, specific energy, specific power, and efficiency in 0.1, 0.5, and 1 M NaOH electrolytes.

### Redox mechanism

The probable mechanism in Scheme 1c demonstrates the reason for longer discharge time and greater Coulombic efficiency than 100%. The  $-\text{CH}=\text{N}-$  electron-withdrawing group present in all the samples of the OTD series plays a vital role in redox reactions on electrodes. The electrode's redox behavior relies on the electron-withdrawing or -donating speed of the  $-\text{CH}=\text{N}$  linkage from the furan moiety. In the charging process, the electron withdrawn from the furan moiety is rapidly donated to a sodium metal electrolyte, while in the discharging process; the electron comparatively

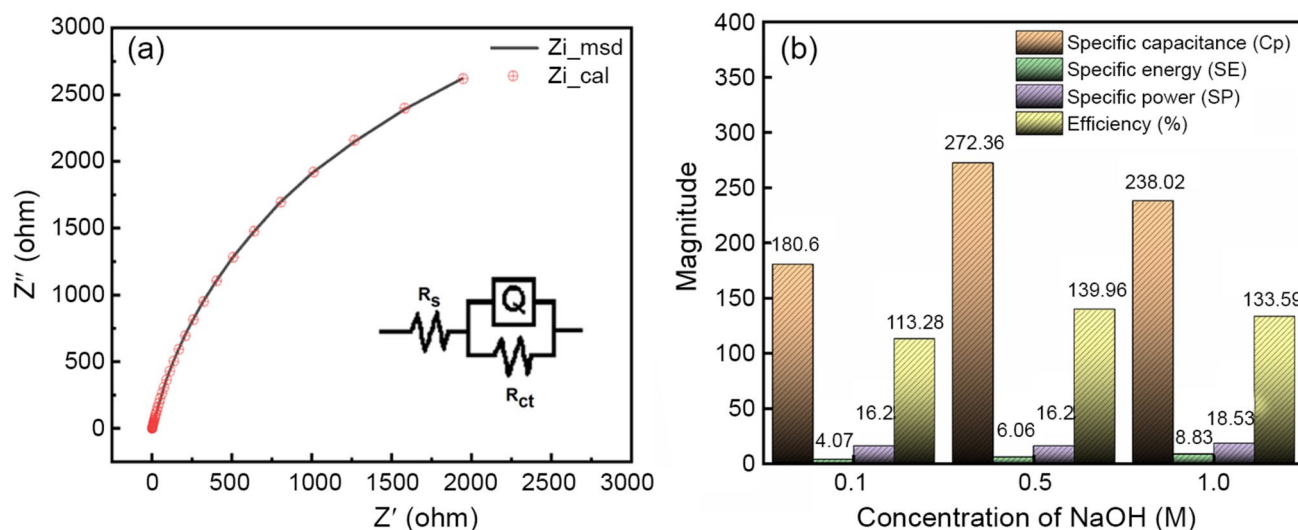


**Fig. 10** **a** Impedance Nyquist plot in 0.5 M NaOH electrolyte (in inset equivalent circuit) and **b** bar diagram for comparison of supercapacitor parameters of OTD-2

slowly withdrawn from the sodium metal is due to the strong bond between electronegative nitrogen and electropositive sodium metal. It is also observed from GCD, as shown in Fig. 8e, that the discharge curve comprises two steps: the initial step shows rapid discharge, and the later step shows slow discharge. In the first half of the steps, the rapid discharge is due to an electron deficiency of furan oxygen, which is partially removed by the hydroxide ion of the electrolyte, and slowing down the discharging process in the latter part. Scheme 1c demonstrates the larger or near 100% Columbic efficiency of polyazomethines.

## Conclusion

We have synthesized a bio-based monomer polyazomethines (OTD) at room temperature using the polycondensation method. The resulting polymers were soluble in organic solvents and exhibited significant bands and atomic peaks, which have been revealed through spectroscopic techniques. XRD analysis revealed that the OTD series possess an amorphous structure. The FESEM image of OTD-2 powder showed granular morphology, while surface wettability measurement tests indicated a  $31.88^\circ$  water contact angle value, which suggested that the electrode has an enhanced capacity for electrolyte ion infiltration and thus more redox reactions can occur over a larger area. In 0.5 M NaOH electrolyte, the OTD electrodes demonstrate a maximum  $C_p$  of  $272.36 \text{ F g}^{-1}$ , an SE of  $6.06 \text{ Whr kg}^{-1}$ , and an SP of  $16.20 \text{ kW kg}^{-1}$ . The stability of OTD-2 is excellent (71.25%). Overall, the elevated supercapacitive character of the OTD electrode is attributed to the easy processing, high

energy density, lightweight, high conductivity, and environmental friendliness of the polyazomethines produced through this method.

**Supplementary Information** The online version contains supplementary material available at <https://doi.org/10.1007/s13726-023-01260-y>.

**Data availability** Data will be made available on request.

## References

- Hajibeygi M, Shafiei-Navid S, Shabanian M, Vahabi H (2018) Novel poly(amide-azomethine) nanocomposites reinforced with polyacrylic acid-co-2-acrylamido-2-methylpropanesulfonic acid modified LDH: synthesis and properties. *Appl Clay Sci* 157:165–176
- Iwan A, Palewicz M, Chuchmała A, Gorecki L, Sikora A, Mazurek B, Pasiać G (2012) Opto(electrical) properties of new aromatic polyazomethines with fluorene moieties in the main chain for polymeric photovoltaic devices. *Synth Met* 162:143–153
- Iwan A (2015) An overview of LC polyazomethines with aliphatic–aromatic moieties: thermal, optical, electrical and photovoltaic properties. *Renew Sust Ener Rev* 52:65–79
- Kou Y, Xu Y, Guo Z, Jiang D (2011) Supercapacitive energy storage and electric power supply using an aza-fused  $\pi$ -conjugated microporous framework. *Angew Chem Int Ed* 50:8753–8757
- Xu F, Chen X, Tang Z, Wu D, Fu R, Jiang D (2014) Redox-active conjugated microporous polymers: a new organic platform for highly efficient energy storage. *Chem Commun* 50:4788–4790
- Matsumoto T, Yamada F, Kurosaki T (1997) Fully conjugated and soluble polyazomethines. *Macromolecules* 30:3547–3552
- Wang Y, Shi Z, Huang Y, Ma Y, Wang C, Chen M, Chen Y (2009) Supercapacitor devices based on graphene materials. *J Phys Chem C* 113:13103–13107
- Salunkhe P, Patil Y, Dhole I, Kalshetti B, Patil V, Mane S, Ghanwat A (2019) A novel synthetic approach for designing metal-free, redox-active quinoxaline-benzimidazole-based

- organic polymers with high energy storage capacity. *New J Chem* 43:14806–14817
9. Manilal M, Sirsendu S, Ritam P, Sukdeb M, Naresh M, Priyabrata B (2020) Efficient tribological properties of azomethine functionalized chitosan as a bio-lubricant additive in paraffin oil: experimental and theoretical analysis. *RSC Adv* 10:33401–33416
  10. Ates M, Kuzgun O, Candan I (2022) Supercapacitor performances of titanium–polymeric nanocomposites: a review study. *Iran Polym J* 31:31–57
  11. Hussein M, Abdel-Rahman M, Asiri A, Alamry K, Aly K (2012) Review on: liquid crystalline polyazomethines polymers basics, syntheses and characterization. *Des Monom Polym* 15:431–463
  12. Hindson J, Ulgut B, Friend R, Greenham N, Norder B, Kotlewski A, Dingemans J (2010) All-aromatic liquid crystal triphenylamine-based poly(azomethine)s as hole transport materials for opto-electronic applications. *J Mater Chem* 20:937–944
  13. Sajid M, Zhao X, Liu D (2018) Production of 2,5-furandicarboxylic acid (FDCA) from 5-hydroxymethylfurfural (HMF): recent progress focusing on the chemical-catalytic routes. *Green Chem* 20:5427–5453
  14. Li Q, Li Y (2023) Self-healable polymer networks from bio-based platform chemicals through Passerini and Diels-Alder reactions: a preliminary study. *Iran Polym J* 32:1307–1319
  15. Uva A, Lin A, Tran H (2023) Biobased, degradable, and conjugated poly(azomethine)s. *J Am Chem Soc* 145:3606–3614
  16. Obushak N, Lesyuk A, Gorak Y, Matiichuk V (2009) Mechanism of Meerwein arylation of furan derivatives. *Russ J Org Chem* 45:1375–1381
  17. Petrus M, Bouwer R, Lafont U, Murthy D, Kist R, Böhm M, Olivier Y, Savenije T, Siebbeles L, Greenham N, Dingemans T (2013) Conjugated poly(azomethine)s via simple one-step polycondensation chemistry: Synthesis, thermal and optoelectronic properties. *Polym Chem* 4:4182–4191
  18. Salunkhe P, Patil Y, Patil V, Navale Y, Dhole I, Ubale V, Maldar N, Ghanwat A (2018) Synthesis and characterization of conjugated porous polyazomethines with excellent electrochemical energy storage performance. *J Polym Res* 25:147
  19. Hafeez A, Akhter Z, Gallagher J, Khan N, Gul A, Shah U (2019) Synthesis, crystal structures, and spectroscopic characterization of bis-aldehyde monomers and their electrically conductive pristine polyazomethines. *Polymer* 11:1448
  20. Li G, Yu K, Noordijk J, Meeusen M, Gebben B, Lohuis M, Schotman M, Bernaerts V (2020) Hydrothermal polymerization towards fully biobased polyazomethines. *Chem Commun* 56:9194–9197
  21. Yuya T, Senri H, Ken-Ichi K (2018) Biobased poly(Schiff-base) composed of bifurfural. *ACS Omega* 3:5336–5345
  22. Patil Y, Mahindrakar J, Salunkhe P, Ubale V, Ghanwat A (2019) Synthesis, characterization, and electrical and thermal stability of semiconducting  $\pi$ -conjugated polyazomethines containing a tetraphenylthiophene-oxazole unit. *J Electron Mater* 48:8067–8075
  23. Li L, Zhang Y, Lu H, Wang Y, Xu J, Zhu J, Zhang C, Liu T (2020) Cryopolymerization enables anisotropic polyaniline hybrid hydrogels with superelasticity and highly deformation-tolerant electrochemical energy storage. *Nat Commun* 11:62
  24. Kulandaivalu S, Suhaimi N, Sulaiman Y (2019) Unveiling high specific energy supercapacitor from layer-by-layer assembled polypyrrole/graphene oxide/polypyrrole/manganese oxide electrode material. *Sci Rep* 9:4884
  25. Patil Y, Salunkhe P, Navale Y, Patil D, Ubale V, Ghanwat A (2020) Tetraphenylthiophene–thiazole-based  $\pi$ -conjugated polyazomethines: synthesis, characterization and gas sensing application. *Polym Bull* 77:2205–2226
  26. Guo R, Qi L, Mo Z (2017) A new route to synthesize polyaniline-grafted carboxyl-functionalized graphene composite materials with excellent electrochemical performance. *Iran Polym J* 26:423–430
  27. Selva M, Bhat D (2009) Polyvinyl alcohol–polystyrene sulfonic acid blend electrolyte for supercapacitor application. *Phys B Condens* 404:1143–1147
  28. Pal B, Yang S, Ramesh S, Thangadurai V, Jose R (2019) Electrolyte selection for supercapacitive devices: a critical review. *Nanoscale Adv* 1:3807–3835
  29. Abdah A, Awan H, Mehar M, Mustafa M, Walvekar R, Alam M, Khalid M, Umapathi R, Chaudhary V (2023) Advancements in MXene-polymer composites for high-performance supercapacitor applications. *J Energ Storage* 63:106942
  30. Kamaci M (2023) Poly(azomethine-urethane)-based fluorescent chemosensor for the detection of  $\text{Cr}^{3+}$  cations in different water samples. *J Fluoresc* 33:53–59
  31. Li Q, Ma C, He Y (2023) Effective one-pot chemoenzymatic cascade catalysis of biobased feedstock for synthesizing 2,5-diformylfuran in a sustainable reaction system. *Bioresour Technol* 378:128965
  32. Salleh N, Kheawhom S, Ashrina N, Rahiman W, Mohamad A (2023) Electrode polymer binders for supercapacitor applications: a review. *J Mater Res Technol* 23:3470–3491
  33. Yang F, Wang D, Zhao Y, Tsui K, Bae S (2018) A study of the relationship between Columbic efficiency and capacity degradation of commercial lithium-ion batteries. *J Energ* 145:486–495
  34. Ko J, Nam J, Won J, Kim K (2014) Supercapacitive properties of electrodeposited polyaniline electrode in acrylic gel polymer electrolytes. *Synth Met* 189:152–156
  35. Zhao C, Zheng W, Wang X, Zhang H, Cui X, Wang H (2013) Ultrahigh capacitive performance from both  $\text{Co}(\text{OH})_2/\text{graphene}$  electrode and  $\text{K}_3\text{Fe}(\text{CN})_6$  electrolyte. *Sci Rep* 3:2986
  36. Inamdar A, Kim Y, Pawar S, Kim J, Im H, Kim H (2011) Chemically grown, porous, nickel oxide thin-film for electrochemical supercapacitors. *J Power Sourc* 196:2393–2397
  37. Wei Y, Luo W, Li X, Lin Z, Hou C, Ma M, Ding J, Li T, Ma Y (2022) PANI-MnO<sub>2</sub> and Ti<sub>3</sub>C<sub>2</sub>T<sub>x</sub>(MXene) as electrodes for high-performance flexible asymmetric supercapacitors. *Electrochim Acta* 406:139874
  38. Zhu Y, Xu H, Tang J, Jiang X, Bao Y (2021) Preparation of ternary composite CF@ $\gamma$ -MnO<sub>2</sub>/PANI material in electrochemical supercapacitors. *J Mater Sci Mater Electron* 32:1–18
  39. Arvizu M, González F, Romero-Galarza A, Rodríguez-Varela F, García C, García-Lobato M (2022) Symmetric supercapacitors of PANI coated RuO<sub>2</sub>/TiO<sub>2</sub> macroporous structures prepared by electrostatic spray deposition. *J Electrochem Soc* 169:020564
  40. Szkoda M, Zarach Z, Trzciński K, Nowak AP (2020) An aqueous exfoliation of WO<sub>3</sub> as a route for counterions fabrication—improved photocatalytic and capacitive properties of polyaniline/WO<sub>3</sub> composite. *Materials* 13:135781
  41. Gottam R, Srinivasan P (2021) Composite electrode material of MoO<sub>3</sub>-MC-SiO<sub>2</sub>-PANI: aqueous supercapacitor cell with high energy density, 1 V and 250,000 CD cycles. *Polym Adv Technol* 32:2465–2475
  42. Zhuo W, Wang Y, Huang C, Deng M (2021) Enhanced pseudocapacitive performance of symmetric polypyrrole-MnO<sub>2</sub> electrode and polymer gel electrolyte. *Polymer* 13:3577
  43. Xue J, Yang Q, Guan R, Shen Q, Liu X, Jia H, Li Q (2020) High-performance ordered porous polypyrrole/ZnO films with improved specific capacitance for supercapacitors. *Mater Chem Phys* 256:123591
  44. He Q, Ye J, Peng Z, Guo Y, Tan L, Chen Y (2021) Electrodeposition of poly(3,4-ethylenedioxythiophene) coated manganese dioxide nanospheres for flexible asymmetric planar

- supercapacitor with superior energy density. *J Power Sourc* 506:230176
45. Shokry A, Karim M, Khalil M, Ebrahim S, El Nady J (2022) Supercapacitor based on polymeric binary composite of polythiophene and single-walled carbon nanotubes. *Sci Rep* 12:11278

Springer Nature or its licensor (e.g. a society or other partner) holds exclusive rights to this article under a publishing agreement with the author(s) or other rightsholder(s); author self-archiving of the accepted manuscript version of this article is solely governed by the terms of such publishing agreement and applicable law.